Rational Doping of P and W in Multi-Stage Catalysts to Trigger Pt-like Electrocatalytic Performances

Yunmei Du[a], Wensi Wang[a], Huimin Zhao[a], Yanru Liu [a, *], Shaoxiang Li [b] and Lei Wang [a, b, *]

a. Key Laboratory of Eco-chemical Engineering, Taishan Scholar Advantage and Characteristic Discipline Team of Eco Chemical Process and Technology, Ministry of Education, Laboratory of Inorganic Synthesis and Applied Chemistry, College of Chemistry and Molecular Engineering, Qingdao University of Science and Technology, Qingdao 266042, P. R. China

b. Shandong Engineering Research Center for Marine Environment Corrosion and Safety Protection, College of Environment and Safety Engineering, Qingdao University of Science and Technology, Qingdao 266042, P. R. China

Experimental Section

1. Electrochemical measurements

Electrochemical measurements toward HER, OER and Overall water splitting were performed by Gamry Instruments Reference 2000 electrochemical station with three-electrode system (include the Hg/Hg_2Cl_2 electrode, a graphite rod and the glassy carbon electrode (SCE) coated with the obtained catalysts). In 1 M KOH, E(RHE)= E(SCE)+0.244 V+0.0592 pH. Generally, the electrochemical property and their conductivity toward HER as well as OER was directly recorded via linear sweep voltammetry (LSV) at 2 mV s^{-1} and Electrochemical Impedance Spectroscopy (EIS) with the frequency range of 0.1~100000 Hz, respectively. To eliminate the influence of uncontrolled resistance of the solution, the LSV curves of HER and OER were iR-corrected with respect to $E_{(iR\text{-}correction)}=E_{(measured)}-I\times R_{(solution)}$. Moreover, TOF was obtained according to the formula: TOF=i/Q and Q=S×A/r=2Fn(HER)=4Fn(OER), where, i=current in Ampere, Q=Quantity of electric charge, A=Geometrical surface area of the electrode, r=scan rate in CV curve, S=the integral area of the CV curve, F=Faraday constant, n=Number of electrons. Notably, the CV test was conducted in 1.0 M PBS (pH=7) at scanning rate of 100 mV s^{-1} in the voltage range of -0.2~0.6V. Meanwhile, C_{dl} was also obtained indirectly through CV test at different scanning speeds. Specifically, CV tests were collected in the non-Faradic region with the scanning speeds of 100~180 mVs^{-1}. Then, according to the linear relationship between Δj and the scanning speed in the obtained CV curve, the C_{dl} value can be collected. The long-time durability test of the P,W-MoS_2/NiSP/NF was operated through using

chronoamperometric (I-T curves) method at the constant potentials of 60 mV for HER and 1.33 V for OER.

2. Characterization

Qualitative analysis and crystal structure of the P,W-MoS_2/NiSP/NF and other contrast samples were implemented on X-ray powder diffraction (XRD) of X'Pert PRO MPD measurement with the scanning rate of 1° min^{-1}. The various morphology theP,W-MoS_2/NiSP/NF and other contrast catalysts carries can be determined by SEM (JEOL, JSM-7500F). EDS data, TEM images as well as its related TEM mapping analysis were obtained by TEM (FEI, Tecnai-C20). Meanwhile, analysis of the electronic state of the external catalysts was gained by XPS test which was conducted on Thermo Scientific Escalab 250Xi.

3. DFT Computational details

All the spin-polarized calculations were performed using the Vienna ab initio simulation package (VASP) version, which is a plane-wave density functional code. The electron–electron exchange and correlation interactions were described by using the generalized gradient approximation (GGA) with the Perdew–Burke–Ernzerhof (PBE) functional form. The projector augmented-wave (PAW) method was employed to describe the interaction between the core and valence electrons. The wave functions were expanded in a plane-wave basis set with a cutoff energy of 400 eV. The convergence criteria for energy and force were 1×10^{-5} eV/cell and 0.02eV/Å. We choose the k-grids of $5 \times 5 \times 1$ point in the full Brillouin zone for our calculation of S-terminated 2H-MoS_2 and the 3×3 sizes 1T-MoS_2 slabs. In order to better

describe the interactions between molecules, van der Waal (vdw) interactions are included descripting by DFT-D_3 method of Grimme.

Figure Captions

Fig. S1 XRD of NiS/NF.

Fig. S2 SEM images of NiS/NF.

Fig. S3 XRD of NiSP/NF.

Fig. S4 SEM images of NiSP/NF.

Fig. S5 Raman spectra of the as-formed MoS_2/NiSP/NF and P, W-MoS_2/NiSP/NF samples.

Fig. S6 XPS spectra of MoS_2/NiSP/NF and NiSP/NF: (a) Ni 2p, (b) S 2p, (c) P 2p.

Fig. S7 LSV curves without iR-compensation for HER in 1.0 M KOH.

Fig. S8 LSV curves without iR-compensation for OER in 1.0 M KOH.

Fig. S9 (a) Post-HER image and (b) Post-OER image of P, W-MoS_2/NiSP/NF.

Fig. S10 (a) XRD pattern and XPS spectra of the P, W-MoS_2/NiSP/NF after HER stability test: (b) Ni 2p, (c) Mo 3d, (d) S 2p and (e) P 2p spectrum.

Fig. S11 (a) Simulated models of P, W-doped 1T- MoS_2 and pure 2H- MoS_2 for formation of intermediates (*H-OH, *H) under HER in KOH solution, (b) the calculated ΔG diagram for HER.

Fig. S12 (a) XRD pattern and XPS spectra of the P, W-MoS_2/NiSP/NF after OER stability test: (b) Ni 2p, (c) Mo 3d, (d) S 2p and (e) P 2p spectrum.

Fig. S13 Cyclic Voltammograms of P, W-MoS_2/NiSP/NF and MoS_2/NiSP/NF in 1.0 M PBS at scanning rate of 100 mV s^{-1}.

Fig. S14 Cyclic voltammograms for (a) MoS_2/NiSP/NF and (b) P, W-MoS_2/NiSP/NF catalysts recorded in 1 M KOH at the voltage rang of 0.1~0.2 V to determine the

double-layer capacitance.

Fig. S15 Cyclic voltammograms for (a) MoS_2/NiSP/NF and (b) P, W-MoS_2/NiSP/NF catalysts recorded in 1 M KOH at the voltage rang of 0.97~1.07 V to determine the double-layer capacitance.

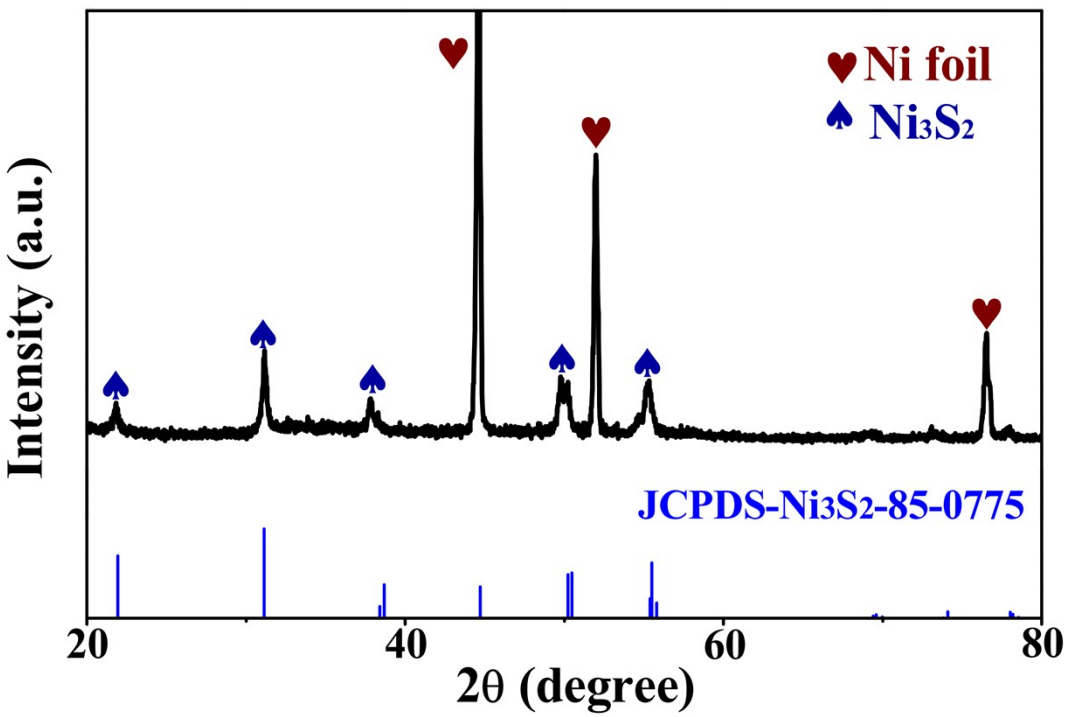

Fig. S1 XRD of NiS/NF.

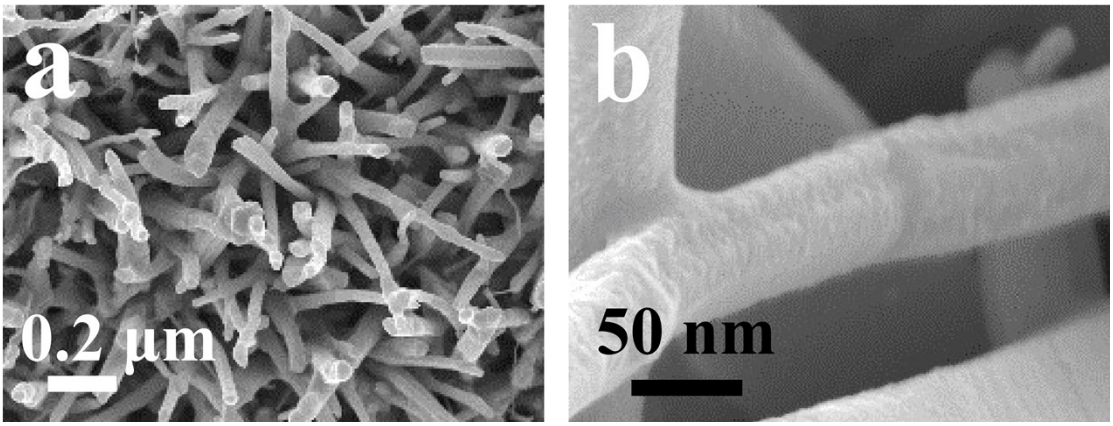

Fig. S2 SEM images of NiS/NF.

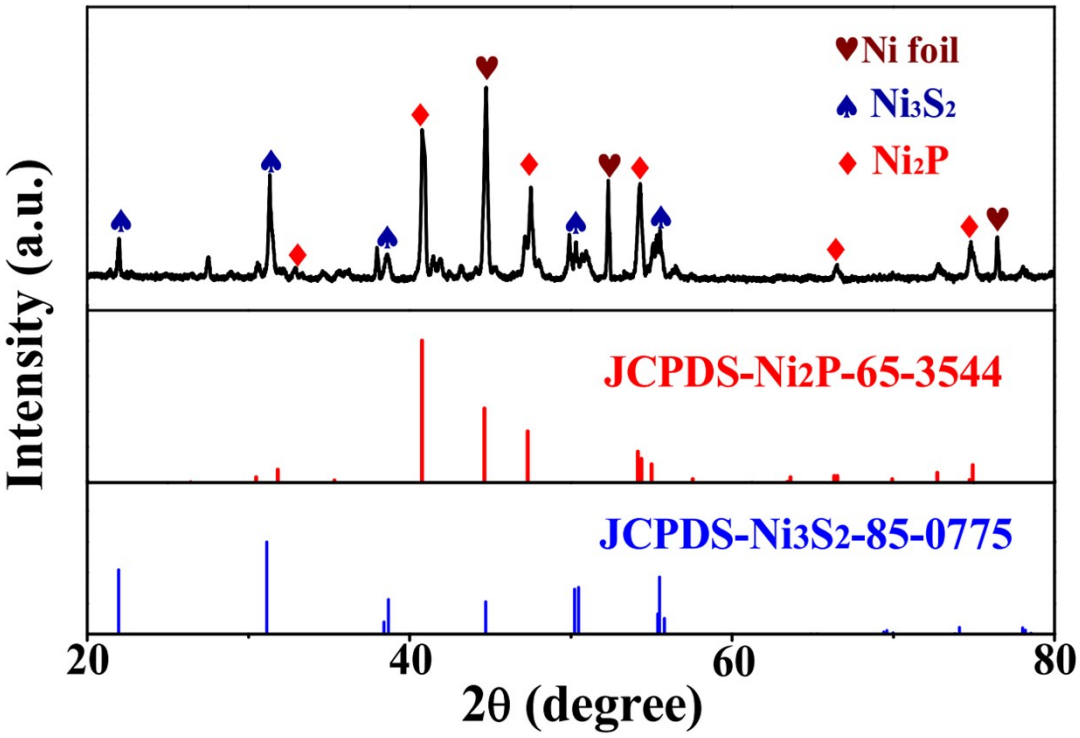

Fig. S3 XRD of NiSP/NF.

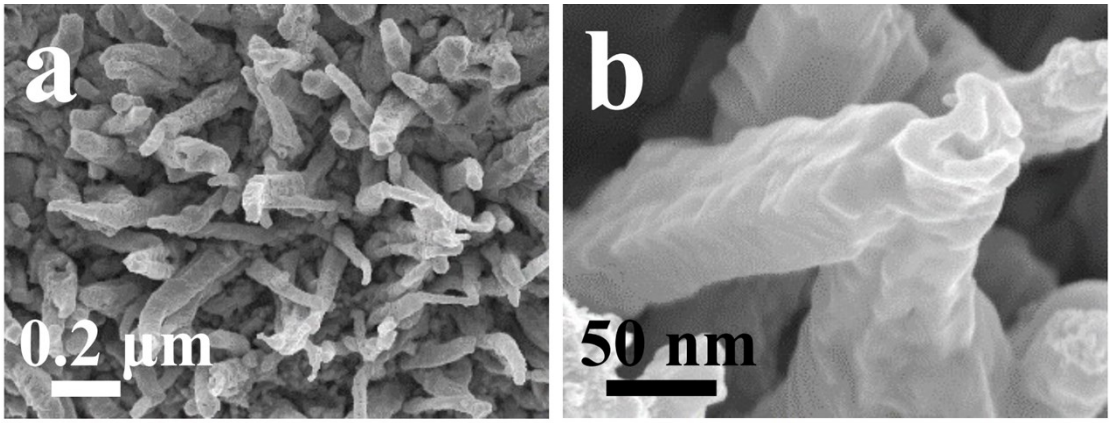

Fig. S4 SEM images of NiSP/NF.

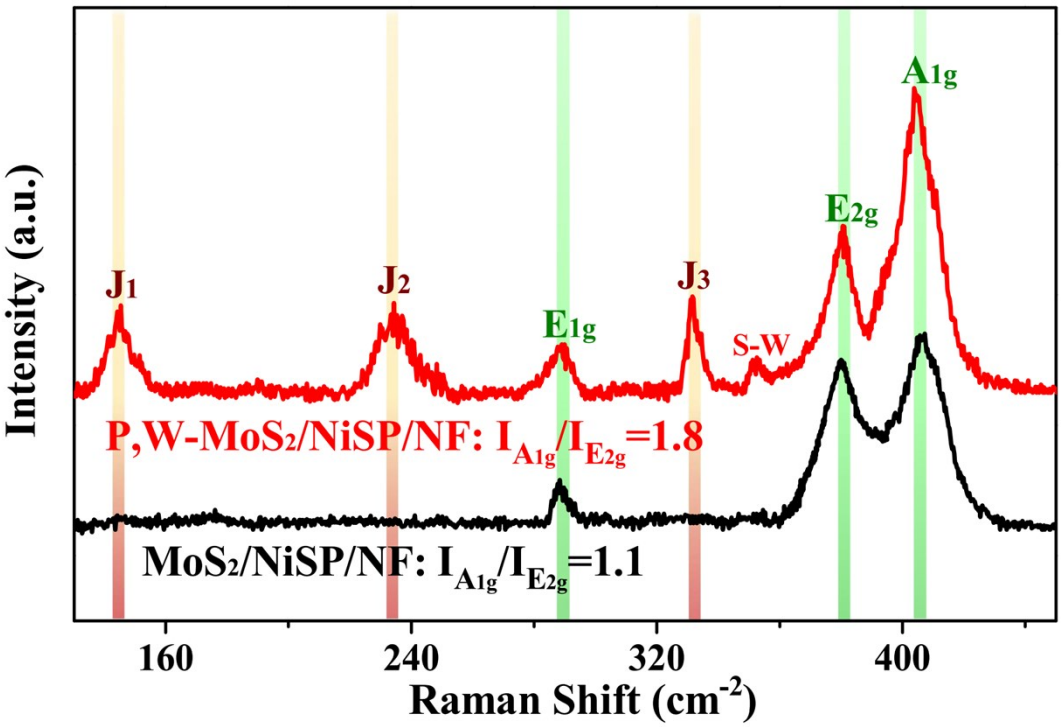

Fig. S5 Raman spectra of the as-formed MoS_2/NiSP/NF and P, W-MoS_2/NiSP/NF samples

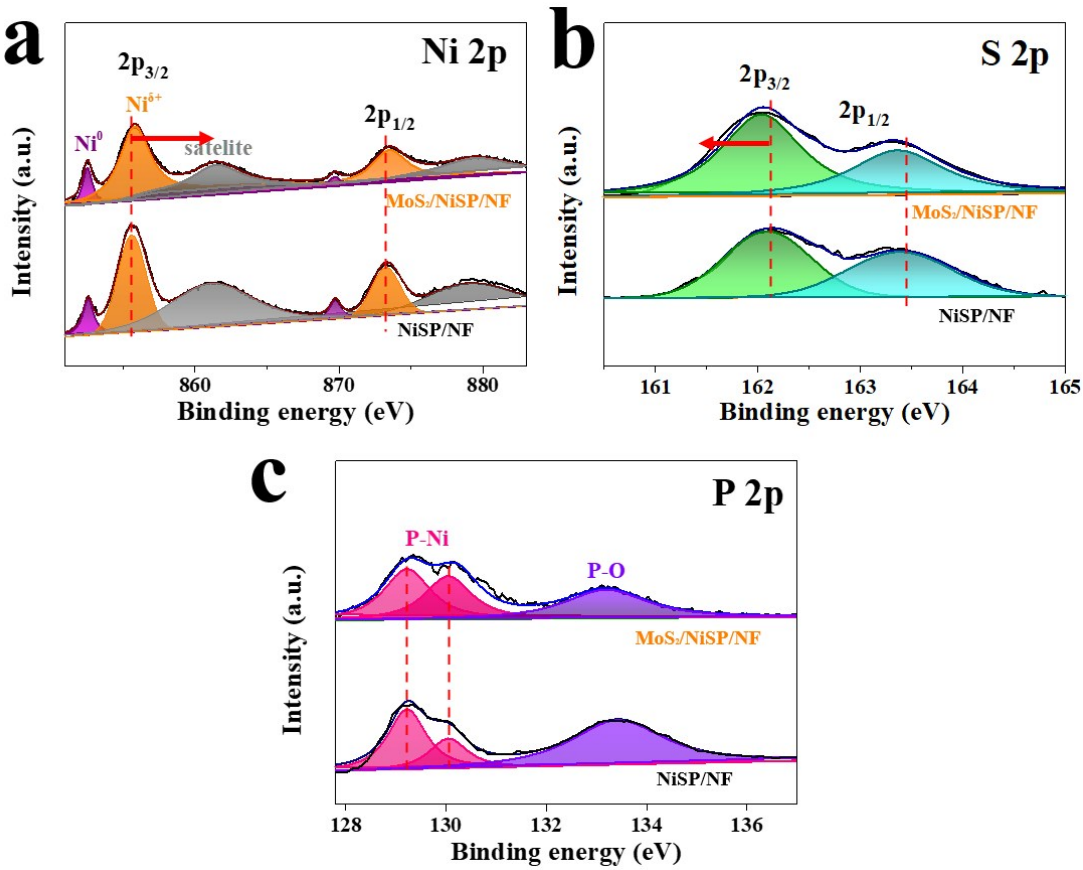

Fig. S6 XPS spectra of MoS_2/NiSP/NF and NiSP/NF: (a) Ni 2p, (b) S 2p, (c) P 2p.

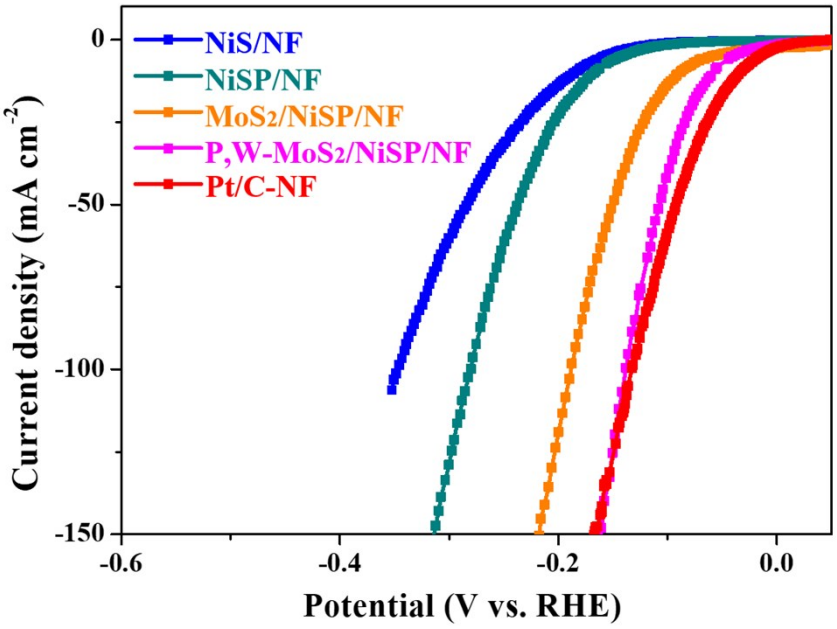

Fig. S7 LSV curves without iR-compensation for HER in 1.0 M KOH**.**

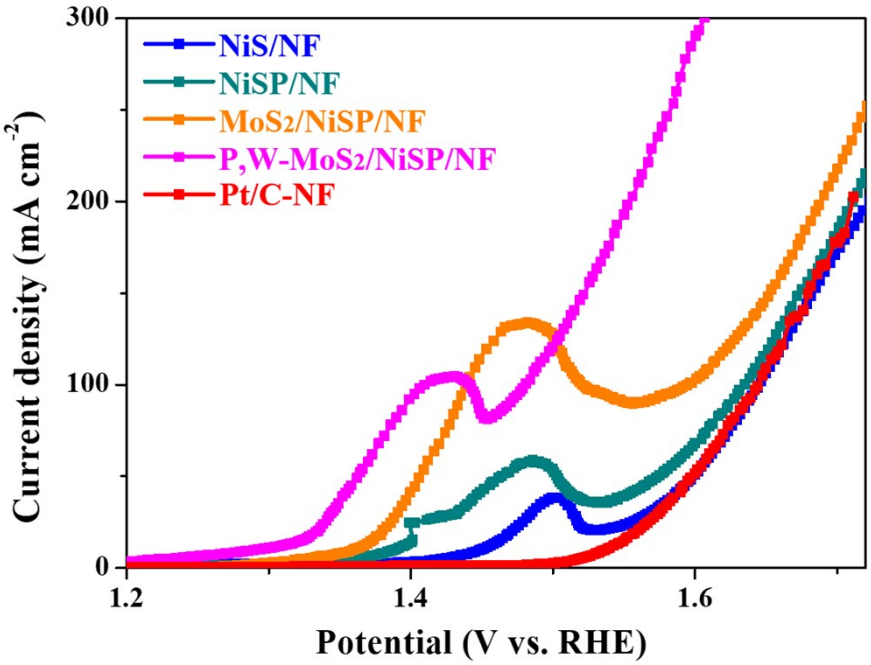

Fig. S8 LSV curves without iR-compensation for OER in 1.0 M KOH.

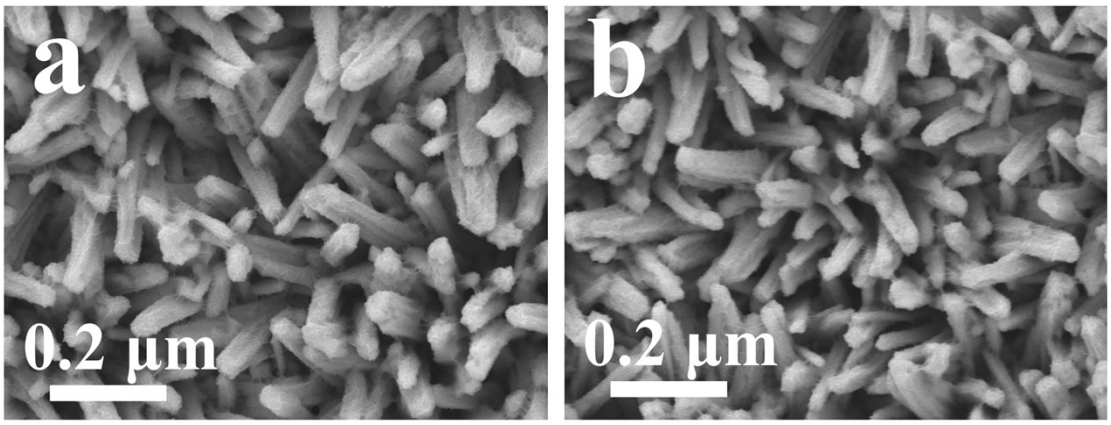

Fig. S9 (a) Post-HER image and (b) Post-OER image of P, W-MoS_2/NiSP/NF.

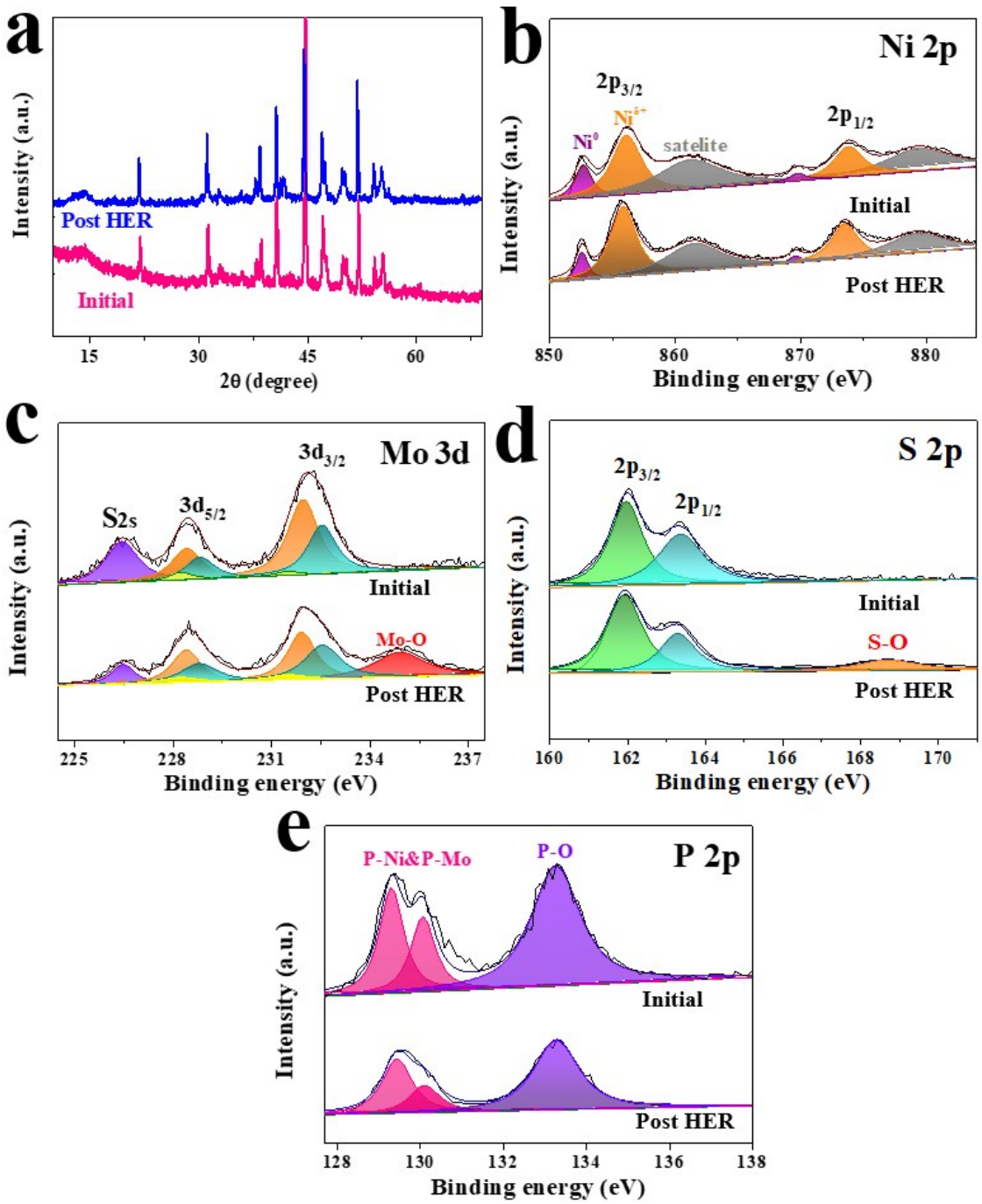

Fig. S10 (a) XRD pattern and XPS spectra of the P, W-MoS_2/NiSP/NF after HER stability test: (b) Ni 2p, (c) Mo 3d, (d) S 2p and (e) P 2p spectrum.

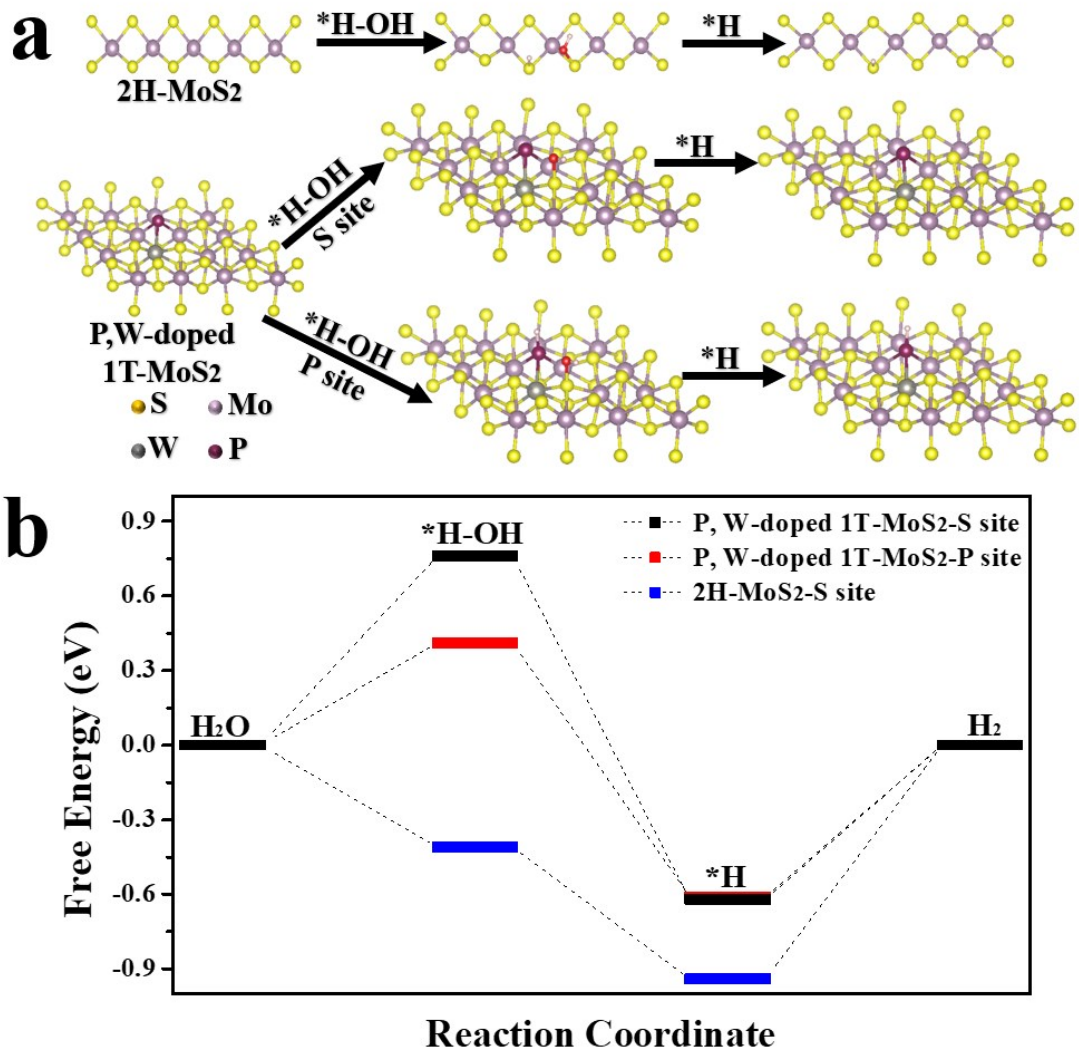

Fig. S11 (a) Simulated models of P, W-doped 1T- MoS_2 and pure 2H- MoS_2 for formation of intermediates (*H-OH, *H) under HER in KOH solution, (b) the calculated ΔG diagram for HER.

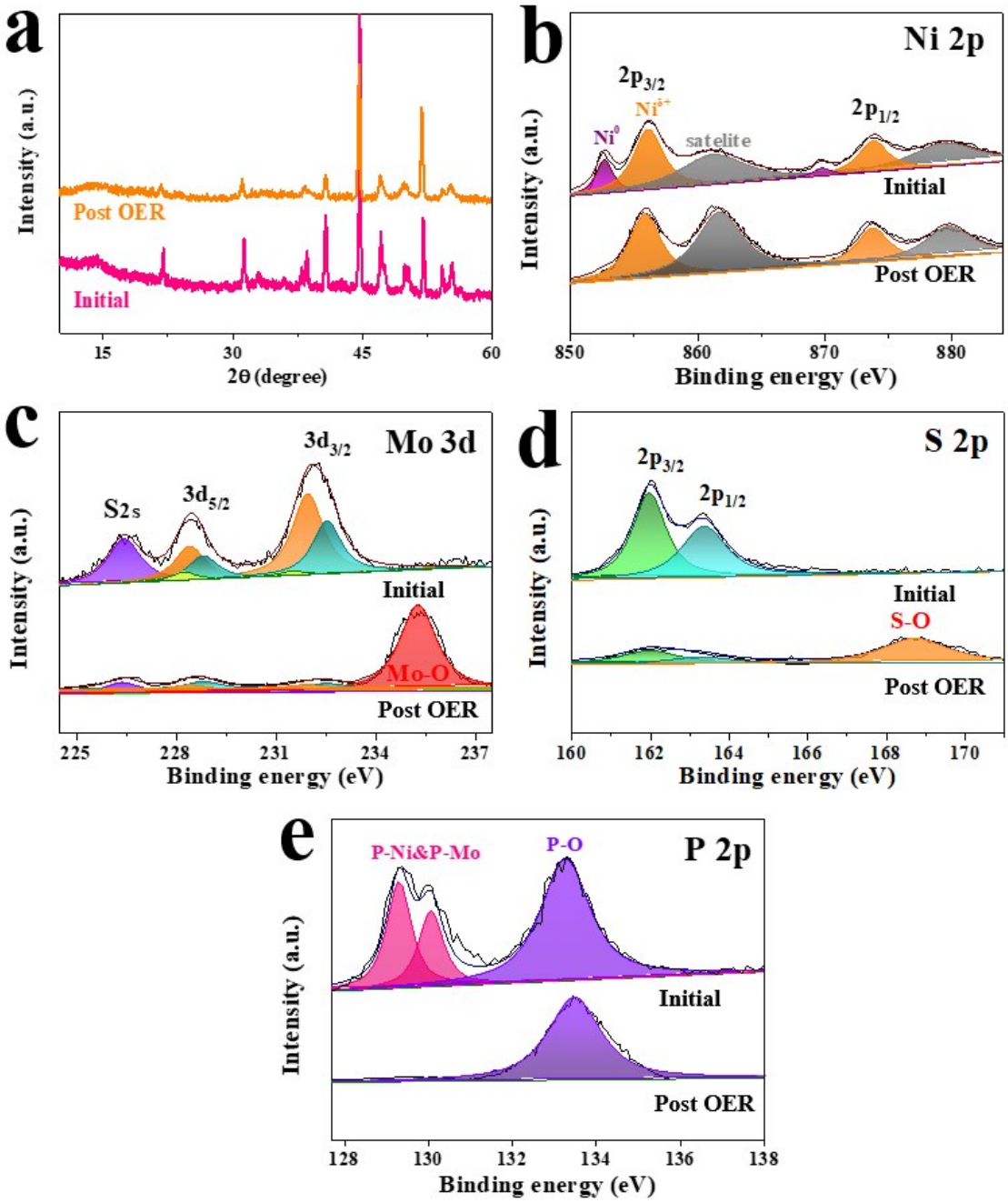

Fig. S12 (a) XRD pattern and XPS spectra of the P, W-MoS_2/NiSP/NF after OER stability test: (b) Ni 2p, (c) Mo 3d, (d) S 2p and (e) P 2p spectrum.

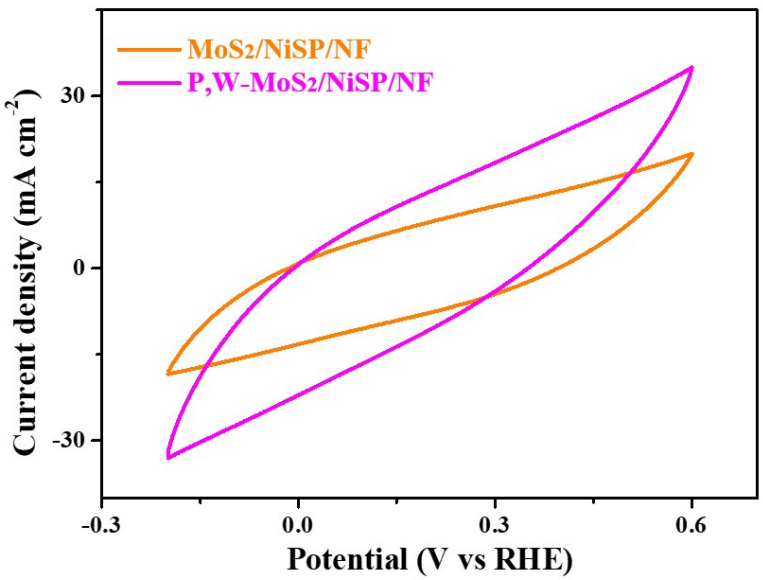

Fig. S13 Cyclic Voltammograms of P, W-MoS_2/NiSP/NF and MoS_2/NiSP/NF in 1.0 M PBS at scanning rate of 100 mV s^{-1}.

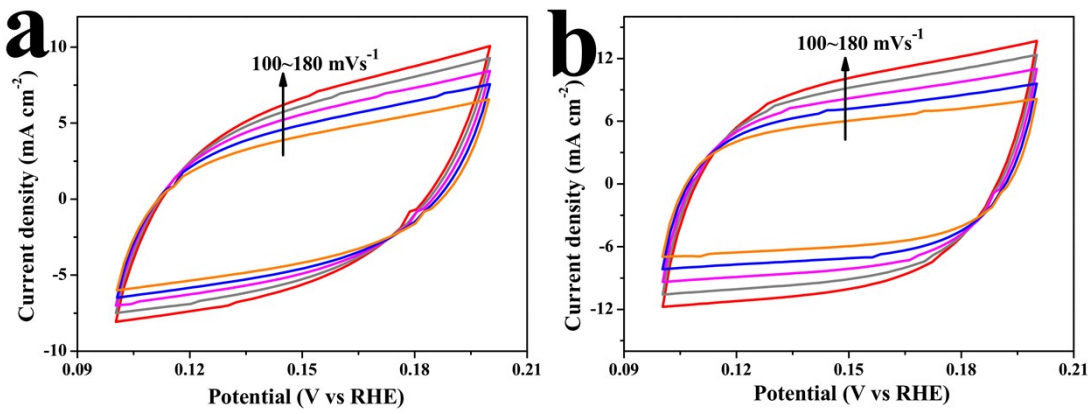

Fig. S14 Cyclic voltammograms for (a) MoS_2/NiSP/NF and (b) P, W-MoS_2/NiSP/NF catalysts recorded in 1 M KOH at the voltage rang of 0.1~0.2 V to determine the double-layer capacitance.

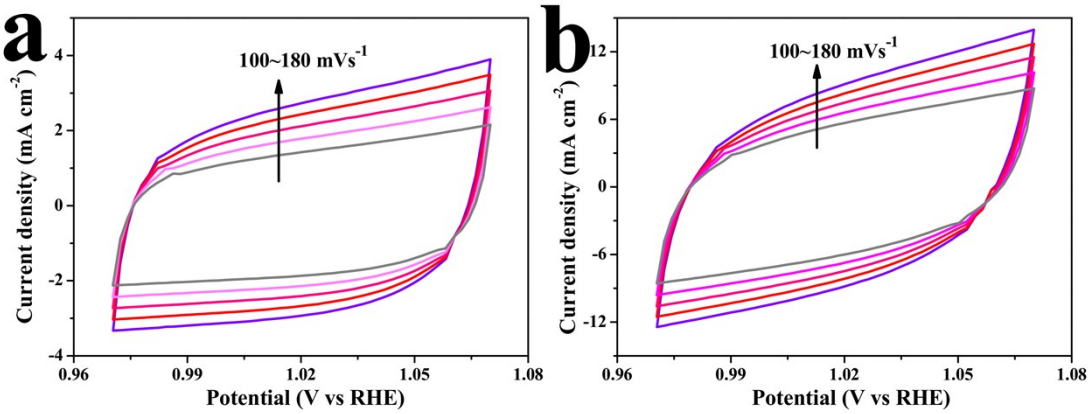

Fig. S15 Cyclic voltammograms for (a) MoS_2/NiSP/NF and (b) P, W-MoS_2/NiSP/NF catalysts recorded in 1 M KOH at the voltage rang of 0.97~1.07 V to determine the double-layer capacitance.